DOI: 10.22281/2413-9920-2026-12-03-246-256

МЕХАНИЧЕСКИЕ ХАРАКТЕРИСТИКИ ГЛИНИСТО-КЕРАМИЧЕСКИХ КОМПОЗИТОВ, АРМИРОВАННЫХ РАКОВИНАМИ УЛИТОК

MECHANICAL PERFORMANCE OF CLAY CERAMIC COMPOSITES REINFORCED WITH SNAIL SHELLS

Аруди И.С.[1], Фергюсон Т.[2], Нурудин А.Х.[1]
Arudi I.S.[1], Ferguson H.T[2], Nurudeen A.H.[1]

[1] – Университет Абуджи (Абуджа, Нигерия)
[2] – Тринити-Колледж Дублина (Дублин, Ирландия)
[1] – University of Abuja (Abuja, Nigeria)
[2] – Trinity College Dublin (Dublin, Ireland)

Аннотация. *Раковины гигантских африканских наземных улиток (GALSS), являющиеся обычными биологическими отходами ресторанов и поставщиков улиток, создают проблемы для окружающей среды из-за неразборчивой утилизации. В предыдущих исследованиях изучалось их применение в медицине, химии, строительстве и автомобилестроении. В данном исследовании изучается введение измельченных галлитов в состав керамических матриц на основе глины для оценки их влияния на механические свойства и пригодности для производства высоковольтных изоляторов. Характерные частицы раковины улитки (63 мкм и 75 мкм) смешивали с глиной в различных пропорциях, формовали в виде брусков и цилиндров, сушили и обжигали при температуре 1200°C. Механические характеристики оценивались с помощью трехточечных испытаний на изгиб и сжатие. Образец 632080 продемонстрировал прочность на изгиб 25,6 МПа, модуль упругости 3,40 ГПа и рассеиваемую энергию 45,04×10*$^{-3}$ *Дж, в то время как образец 752080 продемонстрировал прочность на изгиб 23,3 МПа, 4,05 ГПа и 34,76 × 10*$^{-3}$ *Дж. Плотность чистой глины (C100) составила 24,20 МПа, 3,33 ГПа и 38,32 × 10*$^{-3}$ *Дж. Наибольшая прочность на сжатие (70,5 МПа) была достигнута в образце 752080. Исходя из механических характеристик, оптимальные коэффициенты армирования были определены как 632080 и 752080. Эти результаты свидетельствуют о том, что дробленый галс является экологичным армирующим материалом, обладающим улучшенными свойствами керамического композита и эффективным решением для управления отходами окружающей среды.*

Ключевые слова: *керамика, механические свойства, раковина улитки, композиты.*

Abstract. *Giant African Land Snail shells (GALSs), a common bio-waste from restaurants and snail vendors, pose environmental challenges due to indiscriminate disposal. Previous studies have explored their applications in medicine, chemistry, construction, and automotive industries. This study investigates the incorporation of crushed GALSs into clay-based ceramic matrix composites to evaluate their influence on mechanical properties and assess suitability for high-voltage insulator production. Characterized snail shell particles (63 µm and 75 µm) were blended with clay in varying proportions, molded into bars and cylinders, dried, and fired at 1200 °C. Mechanical performance was assessed through three-point flexural and compression tests. Sample 632080 exhibited a flexural strength of 25.6 MPa, modulus of 3.40 GPa, and energy dissipation of 45.04 × 10*$^{-3}$ *J, while sample 752080 recorded 23.3 MPa, 4.05 GPa, and 34.76 × 10*$^{-3}$ *J. Pure clay (C100) yielded 24.20 MPa, 3.33 GPa, and 38.32 × 10*$^{-3}$ *J. The highest compressive strength (70.5 MPa) was achieved by sample 752080. Based on mechanical performance, optimum reinforcement ratios were identified as 632080 and 752080. These findings highlight crushed GALSs as a sustainable reinforcement material, offering both enhanced ceramic composite properties and a viable solution to environmental waste management.*

Keywords: *ceramics, mechanical properties, snail shells, composites.*

Дата получения статьи:	*15.07.2026*
Дата принятия к публикации:	*24.08.2026*
Дата публикации:	*25.09.2026*

Date of manuscript reception:	*15.07.2026*
Date of acceptance for publication:	*24.08.2026*
Date of publication:	*25.09.2026*

Сведения об авторах:
Аруди Ишиака – PhD, старший преподаватель Департамента механической инженерии Университета Абуджи, Нигерия,
e-mail: shuaibu.ishiaka@uniabuja.edu.ng.

Authors' information:
Ishiaka Arudi – PhD, Senior Lecturer, Department of Mechanical Engineering, University of Abuja, Nigeria, *e-mail: shuaibu.ishiaka@uniabuja.edu.ng*.

DOI: 10.22281/2413-9920-2026-12-03-246-256

Фергюсон Тобинс – PhD, доцент Департамента механической, производственной и биомедицинской инженерии, Тринити-Колледж Дублина,
e-mail: ftobins@tcd.ie.

Нурудин Абдулхаким – PhD (промышленная/производственная инженерия), преподаватель Департамента механической инженерии Университета Абуджи, Нигерия,
e-mail: Hassan.abdulhakeem@uniabuja.edu.ng.
ORCID: https://orcid.org/0000-0002-9624-8224

Tobins Ferguson – PhD, Associate Professor, Department of Mechanical, Manufacturing and Biomedical Engineering, Trinity College Dublin,
e-mail: ftobins@tcd.ie.

Abdulhakeem Nurudeen – PhD in Industrial/Production Engineering, Lecturer, Department of Mechanical Engineering, University of Abuja,Nigeria. *e-mail: Hassan.abdulhakeem@uniabuja.edu.ng.*
ORCID: https://orcid.org/0000-0002-9624-8224

1. Introduction

All technological devices are conceived, engineered, and manufactured through the expertise of engineers; a process fundamentally dependent on the availability of suitable engineering materials. The development of new materials has consistently represented one of the most significant achievements across civilizations, underpinning human progress, prosperity, security, and quality of life throughout history. Indeed, the emergence of novel materials has invariably enabled the advancement of new technologies, spanning disciplines such as civil, chemical, construction, nuclear, aeronautical, agricultural, mechanical, biomedical, and electrical engineering (Buranyi, 2015). The growing demand for advanced materials arises from the need to achieve an optimal balance of strength, toughness, wear resistance, high-temperature performance, and corrosion resistance. In response, researchers are increasingly focused on these properties, often combining two or more constituents to develop novel composites. The present study explores the potential of Giant African Land Snail shells (GALSs) in combination with clay. As technological progress accelerates, the search for new materials becomes imperative, given that conventional options such as common metals and alloys exhibit limitations in attaining desirable mechanical properties. The pursuit of materials with synergistic properties distinct from their individual components has therefore become essential. GALSs have already served as a foundation for research in biology, chemistry, engineering, and medicine (Tobins et al., 2018). Extending their application into engineering contexts aligns with the broader quest to discover and develop innovative materials as shown in Figure 1.

Figure 1. Giant African Snail Shell

2. Literature Review

Research on snail shells has experienced nearly exponential growth over the past decade (Jatto et al., 2010; Ani et al., 2011; Yigezu et al., 2013; Odusanya et al., 2014). However, to the best of the researcher's knowledge, the application of Giant African Land Snail shells (GALSs) as reinforcement in clay-based ceramic matrix composites, and the subsequent effects on their mechanical properties, has not yet been explored. For ceramic insulators used in electric power distribution and transmission systems, the most desirable properties include high dielectric strength, robust mechanical performance, and excellent thermal radiation and insulation capacity, even under humid and corrosive conditions (Adams, 2008). Testing ceramics—whether fiber-reinforced or unreinforced—under pure tension, compression, or shear remains challenging due to their brittle nature, which complicates specimen gripping and uniform loading. Ceramic insulators are essentially ceramic matrix composites, and in this study, the mechanical properties of interest are flexural strength and compressive strength. Other properties such as thermal shock resistance, electrical resistance, dielectric strength (breakdown

DOI: 10.22281/2413-9920-2026-12-03-246-256

voltage), and physical characteristics are addressed in separate works.

Flexural strength

Flexural strength, also known as modulus of rupture, bend strength, or fracture strength, a mechanical parameter for brittle materials, is defined as a material's ability to resist deformation under transverse loads. The transverse bending test is most frequently employed, in which a specimen having either a circular or rectangular cross-section is bent until fracture or yielding using a three-point or a four-point flexural test technique. The flexural strength represents the highest stress experienced within the material at its moment of rupture. It is measured in terms of stress, here given the symbol, σ (Adams, 2008).

In the *bending/flexural test*, a specimen is loaded at one point or two points along its length, under uniaxial bending stress (tension and compression) to obtain information on the bending behaviour of materials, making the test very easy to perform. This explains why it is used for ceramic matrix composites and other brittle materials such as hard metals, tool steels and grey cast iron (Barrata, 1998; Adams, 2008). Generally, a flexure test is designed to measure the bend strength of a brittle material, whereas a bend test is designed to measure the crack resistance of a ductile material (Barrata, 1998; Adams, 2008).

A flexural specimen simply rests on two supports and is loaded at one point, known as the 3-point flexural test or at two points, the 4-point flexural test (Figures 2 and 3). The sample is loaded until it is completely ruptured allowing for the determination of the sample's maximum bend strength.

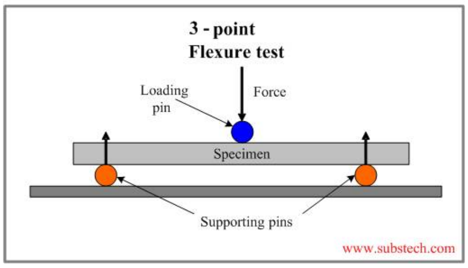

Figure 2. The Three-point Flexural Test (Kopeliovich, www.substech.com)

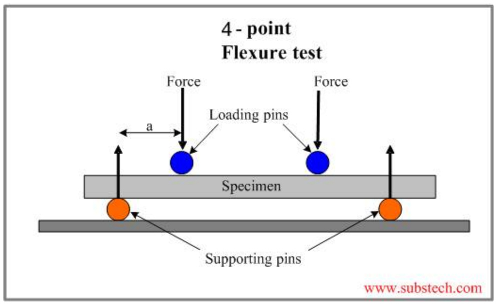

Figure 3. The Four-point Flexural Test (Kopeliovich, www.substech.com)

The flexural strength of brittle materials is very sensitive to the surface finish since the maximum tensile stress occurs on the beam surface. Adams (2008), therefore recommended rounding or bevelling of the corner to avoid stress concentration and to reduce premature failure. ASTMC 1161 C is the primary governing standard for flexural testing of ceramics (Adams, 2008). He also stated the ASTM C 1341 allows a range of specimen sizes and support span-to-specimen thickness ratios. ISO 14125 is the leading non-ASTM standard, and, like ASTM D 7264, it is focused specifically on composite materials and presents relatively concise guidelines and test conditions ((Quinn and Morrel 1991; Adams, 2013). The specimen dimensions according to ASTM D 7264 could be 128mm x 13mm x 4mm for 3-point and 4-point flexural tests. The standard ASTM D790-93, 1998 was suggested by Barrata (1998) for flexural testing for ceramic materials.

3. Methodology

3.1. Materials

Snail shells and fireclay served as the precursor materials for this study. The shells were obtained from the Giant African Land Snail (*Achatina fulica*; class Gastropoda, family Achatinidae), collected from refuse sites and restaurants in the Kugbo Clan and Port Harcourt areas of Rivers State, Nigeria. Commercially processed fireclay, consisting of a proprietary shale-fireclay blend, was sourced from Goodwins Build & DIY Products (Dublin) under the trade name "DINEEN CLAY MIX." The baseline analytical profile of this clay is presented in Table 1.

DOI: 10.22281/2413-9920-2026-12-03-246-256

Table 1
The analysis of the Dublin clay as supplied by BUILD & DIY PRODUCTS'

S/N	Clay mix constituents	Percentage (%)
1	Al_2O_3	25
2	SiO_2	63
3	Fe_2O_3	7.5
4	K_20	2.5
5	Na_2O	1.4
6	MgO	0.4
7	CaO	0.2
Total		100

Pre-incorporated with 12 wt.% fired grog of matching composition. Composed of hydrous aluminum silicates, this refractory clay exhibits high thermal stability, featuring a minimum service temperature of 1515 °C and a fusion point superior to 1600 °C.

3.2. Experimental Methods

3.2.1. Processing and Sieve Analysis

Post-collection, the GALSs were processed at the University of Abuja's Faculty of Engineering workshop. The shells were soaked in water overnight, washed thoroughly with a surfactant solution to remove impurities, and subsequently sun-dried for three days to achieve complete dehydration shown in Figure 4.

Figure 4. The snail shells being dried under the sun

The dried ground African land snail shells (GALSs) were mechanically comminuted using a hammer mill to obtain particles of varying sizes. The resulting fragments were subjected to particle size classification through a sieve analysis in accordance with the BS 410 standard. A series of sieves with apertures of 2000 µm, 1180 µm, 600 µm, 425 µm, 300 µm, 212 µm, 150 µm, 75 µm, and 63 µm were arranged sequentially on a sieve shaker. The assembly was operated under continuous vibration for 20 minutes to ensure effective separation. Following the analysis, the fractionated particles were collected, bagged according to their respective size ranges, and subsequently transported to Trinity College Dublin for further experimental investigation.

3.3. Material Characterization

The crushed ground African land snail shells (GALSSs) and clay fractions with particle sizes below 150 µm were subjected to microstructural and compositional characterization. Scanning Electron Microscopy (SEM) was performed at the Irish Centre for Research in Applied Geosciences (iCRAG), Trinity College Dublin, to examine surface morphology and microstructural features. In addition, both materials were analyzed to determine their chemical compositions, providing insight into their elemental and mineralogical constituents.

3.4. Samples for Flexural and Compressive Tests

Rectangular specimens for flexural and compressive strength testing were prepared using a mould with internal dimensions of 90 mm × 14 mm × 7 mm (Figure 5). The preparation procedure followed the guidelines specified in ASTM C1161-18 (Quinn and Morrel, 1991) for flexural testing of advanced ceramics and ASTM D790-93 (Barrata, 1998) for flexural properties of plastics.

Specimens were prepared for mechanical and physical property evaluation, including flexural strength, fracture toughness, impact strength, thermal shock resistance, and dielectric breakdown voltage. Additional determinations included shrinkage, water absorption, porosity, and bulk density.

DOI: 10.22281/2413-9920-2026-12-03-246-256

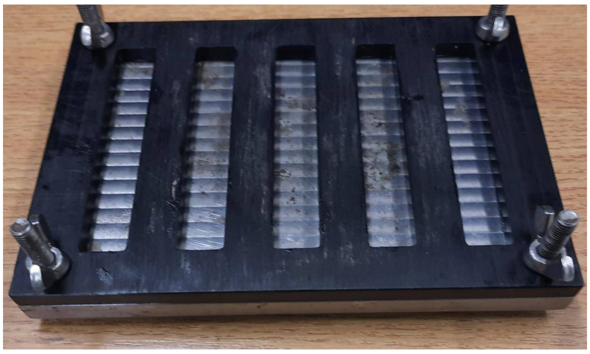

Figure 5. The mould for five samples, each 90mm x 14mm x 7mm.

Crushed ground African land snail shells (GALSSs) were blended with clay in varying proportions, as outlined in Table 2. For example, to obtain a 10:90 mixture (10% GALSSs: 90% clay), 10 g of GALSSs particles (<63 µm) were combined with 90 g of clay particles (<120 µm). Approximately 20–25 mL of water was added to the dry mixture to achieve a homogeneous plastic consistency. The mixture was compacted into a mould (90 mm × 14 mm × 7 mm) by ramming and allowed to set for 12 hours. The resulting greenware bars were removed from the mould and oven-dried at 250 °C for one hour to eliminate residual moisture.

Baseline specimens composed of 100% clay were also prepared. All samples were subsequently fired at temperatures between 1100 °C and 1200 °C to ensure densification and phase development.

Table 2

Samples prepared according to GALSs/clay ratios and particle size

S/N	Particle Size (µm)	GALSs and CLAY Ratios			Total
		10/90	20/80	30/70	
1	-63µm	10	10	10	30
2	63µm	10	10	10	30
3	75µm	10	10	10	30
4	150 µm	10	10	10	30
5	C100 100% clay)				30
Total		40	40	40	150

Cylindrical ceramic matrix composite specimens for compression testing were prepared in accordance with ASTM C1424−15 (2019), employing test methods specified in ASTM C773. The samples were fabricated with dimensions of 30 mm in length and 15 mm in diameter (Figure 6). The preparation procedure was analogous to that used for flexural test specimens, except those cylindrical moulds were employed in place of rectangular ones.

Figure 6. The mould for cylindrical samples for compression tests

Following moulding, the greenware specimens were oven-dried at 250 °C for one hour to remove residual moisture. Subsequently, the dried samples were fired at temperatures ranging from 1100 °C to 1200 °C to achieve densification. Figure 7 illustrates both rectangular and cylindrical specimens after drying, prior to firing.

Figure 7. Rectangular and cylindrical samples arranged and ready for firing

Selected rectangular specimens (Figure 7) were subjected to three-point flexural testing using an Instron 3366 universal testing machine. The tests were conducted to determine the flexural strength, flexural modulus, and energy dissipation during deformation of the ceramic matrix composites. The procedure followed standard protocols to ensure reproducibility and accuracy of mechanical property evaluation.

The flexural strength, flexural modulus, and energy dissipation (quantified as the area under

DOI: 10.22281/2413-9920-2026-12-03-246-256

the load–deflection curve) were determined from the raw data generated by the Instron 3366 testing machine. For the three-point bending tests conducted on rectangular specimens, the flexural strength (σ_f, MPa) was calculated using the following expression:

$$\sigma_3 = \frac{3LF}{(2bd^2)} \quad (1)$$

where P is the maximum applied load (N), L is the span length (mm), b is the specimen width (mm), and d is the specimen thickness (mm).

The flexural modulus was obtained from the slope of the initial linear portion of the load–deflection curve, while the energy dissipated during deformation was determined by integrating the area under the curve up to fracture.

The compressive strength (CS) of the ceramic matrix composites was determined by dividing the maximum applied load at failure (F) by the original cross-sectional area (A) of the specimen:

$$CS = \frac{F}{A} \quad (2)$$

where CS is compressive strength (MPa), F is maximum load at failure (kN), A is initial cross-sectional area of the specimen (mm^2).

For cylindrical specimens, the cross-sectional area was calculated as:

$$A = \frac{\pi d^2}{4} \quad (3)$$

with d representing the diameter of the sample after firing. In this study, the fired diameter was 14 mm, yielding an area of 153.94 mm^2. Accordingly, the compressive strength for all cylindrical samples was expressed as:

$$CS = \frac{F}{153.94} \quad (4)$$

This formulation ensured consistency across all tested specimens.

4. Results and Discussions

4.1. Flexural and Compressive Tests Results

The results of the flexural tests are presented in the order in which they were conducted. The initial series of experiments involved specimens fired at a temperature of 1100 °C, with the objective of evaluating the influence of firing conditions on flexural strength, flexural modulus, and energy dissipation. A subsequent series was performed on samples subjected to firing temperatures ranging from 1130 °C to 1200 °C, aimed at identifying the optimum operational temperature. Finally, tests were conducted on specimens fired at 1200 °C to determine which sample exhibited the most favorable mechanical properties under that condition.

The results obtained from individual specimens are presented in Figures 8 and 9, organized according to the particle size of the GALSs, the GALSs-to-clay ratio, and the firing temperature. For example, the designation "–63 1090 1100" refers to a specimen prepared with GALSs of –63 µm particle size, a GALSs/clay ratio of 10:90, and subjected to firing at 1100 °C. The curve reaches a maximum load of approximately 65–70 N at an extension of around 0.4mm. This peak represents the ultimate load-bearing capacity of the specimen. Beyond this point, the material can no longer sustain additional stress, marking the onset of failure. Following the peak, the curve drops sharply, indicating a sudden loss of load-bearing ability. This steep decline is characteristic of brittle fracture, where crack propagation occurs rapidly once the critical stress threshold is exceeded. Representative load–extension curves exhibiting similar profiles were also illustrated in Figures 10 and 11.

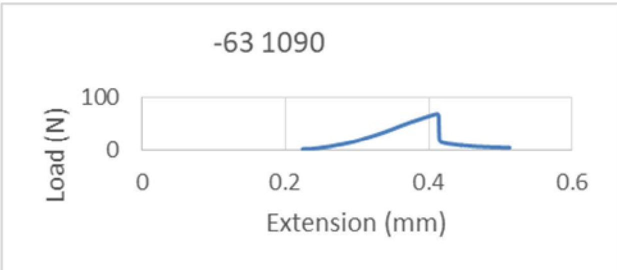

Figure 8. The load-extension curves of sample -631090

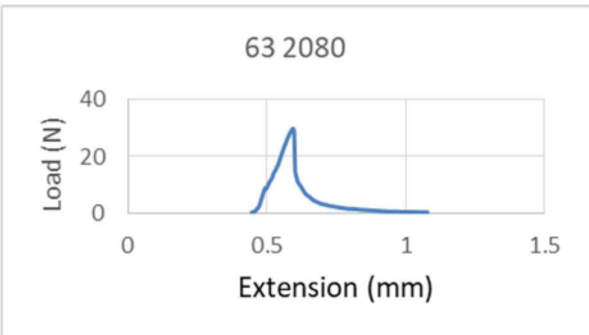

DOI: 10.22281/2413-9920-2026-12-03-246-256

Figure 9. The load-extension curves of sample 632080

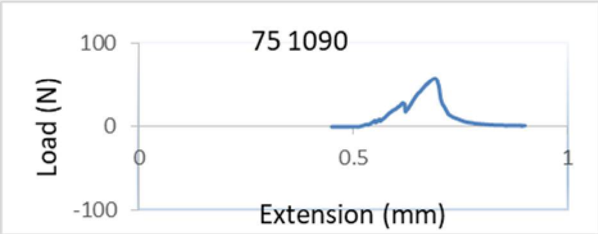

Figure 10. The load-extension curves of sample 751090

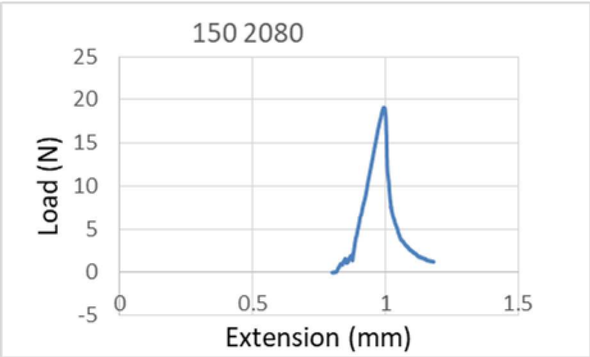

Figure 11. The load-extension curves of sample 1502080

Figure 10 presents the load–extension curve of the specimen composed of 100% clay and fired at 1100 °C. The profile of this curve differs markedly from the others, indicating brittle failure following the appearance of a plateau-like feature. This suggests that, during deformation, the material required additional energy input to progress toward fracture. In contrast, the incorporation of GALSs altered the fracture behavior of the ceramics, as evidenced by the absence of brittle failure in the curves shown in Figures 10 and 11 at the same firing temperature. The calculated values of flexural strength (MPa), flexural modulus (GPa), derived from Equations 1 and 2, together with the energy dissipated during deformation (J), represented by the area under the curves, are summarized in Table 3 and illustrated in Figure 12.

Table 3

GALSs Particle size 63 µm fired at 1100°C

S/N	Sample GALS: Clay	Max load (N)	Flexural strength (MPa)	Flexural modulus (MPa)	Area under curve (N-m)x10^{-3}
1	10:90	43.81	4.12	139.11	3.30
2	20:80	29.87	2.81	180.43	3.15
3	30:70	13.21	1.24	52.84	2.13
4	40:60	7.58	0.74	70.10	1.17
REF: 0:100		135.51	12.77	700.60	24.75

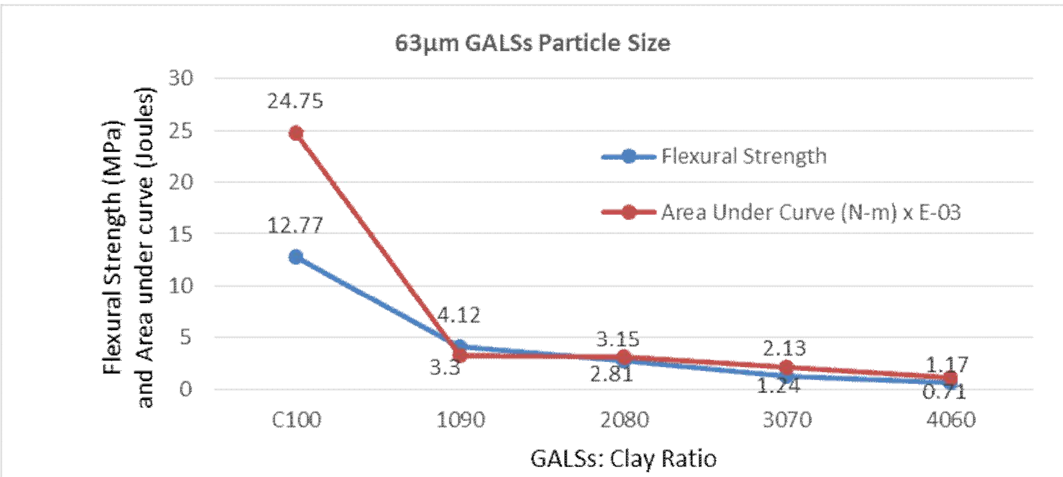

Figure 12. Graph of flexural strength and area under curve (energy) against ratio for 63 µm GALSs particle size with 100% clay

Научно-технический вестник Брянского государственного университета, 2026, №3
Nauchno-tekhnicheskiy vestnik Bryanskogo gosudarstvennogo universiteta, 2026, No.3
DOI: 10.22281/2413-9920-2026-12-03-246-256

The load–displacement curves for specimen 63 1090 subjected to varying firing temperatures are presented in Figures 14–18. The corresponding values of maximum load at fracture, flexural strength (MPa), flexural modulus (GPa), and energy dissipated (J) are summarized in Table 4. Figure 16 illustrates the influence of firing temperature on the ceramic matrix composite for specimen 63 1090. Representative load–displacement curves for the clay-only specimens (C100) are shown in Figures 14 and 15, with the associated mechanical properties reported in Table 4. The effect of firing temperature on the 100% clay ceramics is depicted in Figure 13. Overall, the results demonstrate a consistent increase in maximum load at fracture, flexural strength, flexural modulus, and energy dissipated during deformation as firing temperature increases.

Table 4

The effect of firing temperature on Sample 63 1090

S/N	Firing temperature (ºC)	Max load (N)	Flexural strength (MPa)	Flexural modulus (MPa)	Area under curve (N-m)x10^{-3}
1	1130	54.28	5.11	1528.93	5.22
2	1160	110.83	10.44	2263.87	26.20
3	1180	156.69	14.76	3479.92	31.75
4	1190	165.15	15.56	3023.42	29.93
5	1200	176.58	16.63	3632.10	29.20

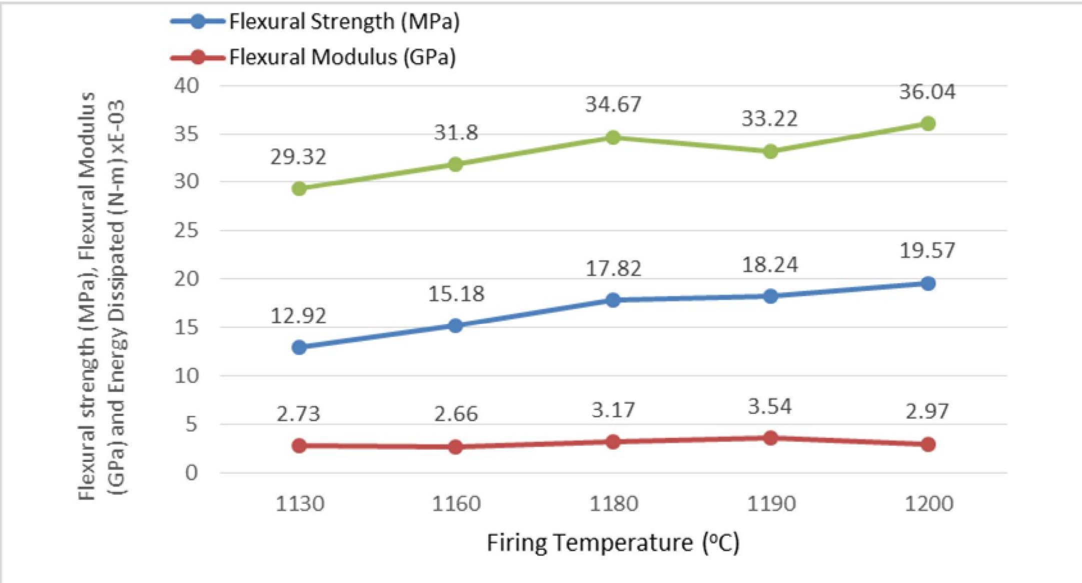

Figure 13. The effect of firing temperature on the ceramic sample C100 (100% clay)

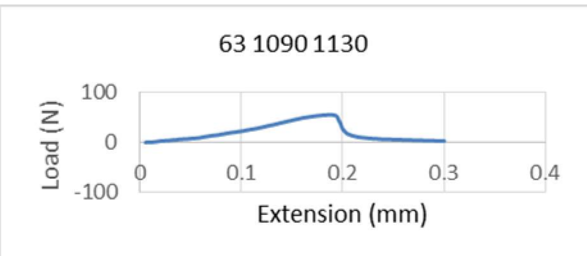

Figure 14. Load-extension graphs of flexural test for samples 6310901130 at 1130ºC

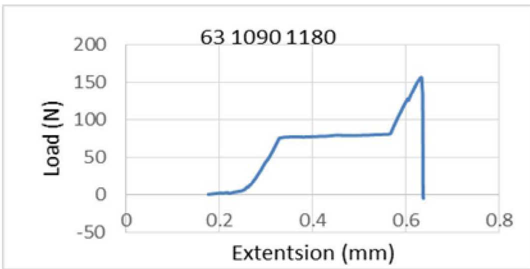

Figure 15. Load-extension graphs of flexural test for sample 6310901180 at 1160ºC

DOI: 10.22281/2413-9920-2026-12-03-246-256

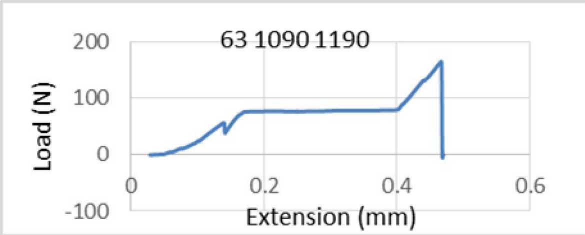

Figure 16. Load-extension graphs of flexural test for sample 6310901180 at 1180ºC

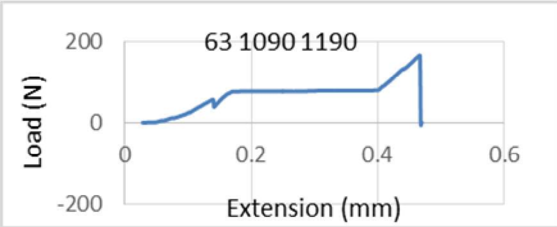

Figure 17. Load-extension graphs of flexural test for sample 6310901180 at 1190ºC

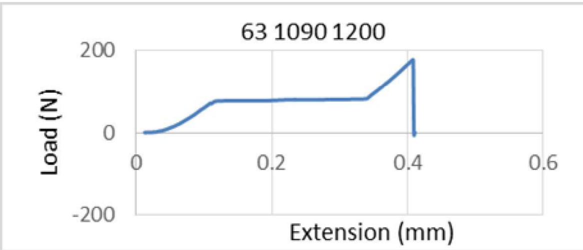

Figure 18. Load-extension graphs of flexural test for samples 63 µm with firing temperature 1200ºC

4.2. Compressive Tests Results

The load–displacement diagrams obtained from the compression tests of selected specimens are presented in Figure 19, categorized according to the GALSs-to-clay ratio and the particle size of the GALSs.

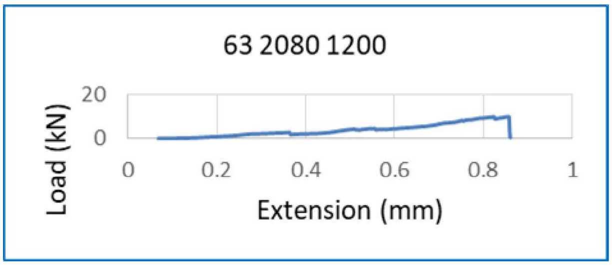

Figure 19. Load-extension graphs of compression tests for sample 63 20801200

The mechanical properties of the ceramic matrix composites namely flexural strength, flexural modulus, and energy dissipation exhibited progressive improvement with increasing firing temperature. A characteristic plateau region was observed in all load–deformation curves (Figures 19-21) for specimen 63 1090 fired between 1160 °C and 1200 °C, resembling the behaviour of the clay-only specimens (Figure 11). During deformation at approximately 80 N loading, additional energy was required for the process to continue, suggesting residual load resistance at this stage. For specimen 63 1090 fired at 1200 °C, the maximum load attained was 176 N, with a flexural strength of 16.63 MPa, a flexural modulus of 3.63 GPa, and energy dissipation of 29.20×10^{-3} J. In contrast, the flexural modulus of the clay-only specimens remained consistently around 3 GPa across all firing temperatures.

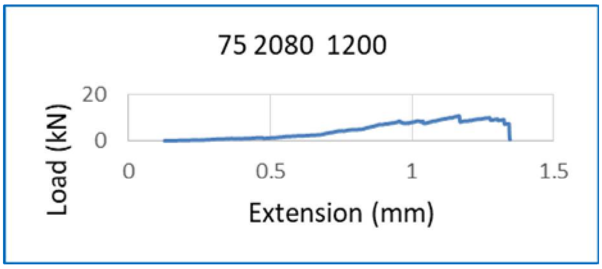

Figure 20. Load-extension graphs of compression tests for sample 75 2080 1200

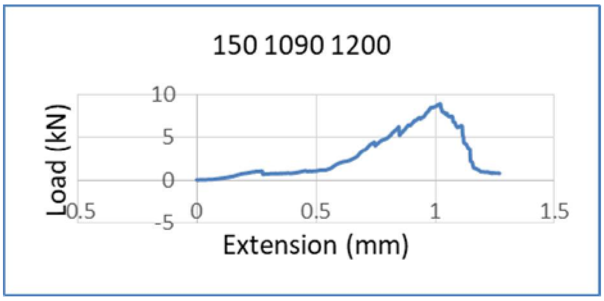

Figure 21. Load-extension graphs of compression tests for sample 150 1090 1200

Firing transformed the ceramic material from a weak, unfused state into a strong, permanent structure. As furnace temperature increased, significant microstructural changes occurred within the ceramics. According to the kiln firing chart (Hall, 2014), clay begins vitrification between 1100 °C and 1200 °C, corresponding to cone numbers 03–01 and 2–5. Within this range, particles begin to melt and crystallize, leading to shrinkage, densification, and hardening, which collectively enhance the maximum load capacity with rising firing temperature. Furthermore, extended soaking time at peak firing temperature facilitated greater particle fusion, thereby improving the mechanical integrity of the ceramics.

Table 5 presents the maximum load, compressive strength and the energy dissipated during the compression tests while Figure 21 shows how the samples of different particle size and GALSs/clay ratios relate with the compressive strength and the energy dissipated.

Table 5

Results of compression tests of selected samples

S/N	Sample	Max load (N)	Compression strength (GPa)	Area under curve (N-m) Joules
	C100	7688	49.94	3.75
1	- 63µm 1090	8509	55.27	2.13
2	63µm 2080	10029	65.15	2.85
3	75µm 2080	10830	70.48	5.15
4	150µm 1090	8790	58.27	3.11

5. Conclusions

The load–deflection curves obtained from compression testing (Figure 13) exhibit distinct characteristics compared to those recorded during flexural testing. Whereas flexural curves generally display smooth profiles, the compression curves reveal irregularities, likely attributable to the presence of multiple yield points during crushing. As illustrated in Figure 14, both compressive strength and energy dissipation increased with higher GALS content and larger particle size, attaining values of 70.48 MPa and 5.15 J, respectively, for specimen 75 µm 2080. On average, the energy dissipated during compression was approximately 3.40 J. In comparison, the clay-only specimen (C100) exhibited a compressive strength of 49.94 MPa and energy dissipation of 3.75 J. Elevated firing temperatures (1200 °C) promoted phase development, densification, and reduced porosity. However, higher GALS content (20%) introduced additional porosity, underscoring the need for careful control of firing conditions to optimize mechanical performance. The most favorable balance of mechanical strength and thermal stability was observed in specimen 632080. Accordingly, mixtures corresponding to specimens 631090 and 632080 are recommended for achieving optimum results.

References

1. Tassew, S. T. (2014). Structural Behaviour of Textile and Steel Reinforced Ceramic Composite Slabs.

2. Ani, J. U., Menkiti, M. C., & Onukwuli, O. D. (2011). Coagulation-flocculation performance of snail shell biomass for waste water purification. *NY Sci J*, *4*(2), 81-90.

3. Aravind, K. A., Poomalai, R. et al (2019). Flashover Performance of Composite and Porcelain Insulators. *February 2019 International Conference on High Voltage Engineering and Technology (ICHVET).*

4. Kolawole, M. Y., Aweda, J. O., Abdul-Kareem, S., Bello, S. A., Ali, A., & Iqbal, F. (2020). Influence of calcined snail shell particulates on mechanical properties of recycled aluminium alloy for automotive application. *Acta Periodica Technologica*, (51), 163-180.

5. ASM D149 − 09 Calcara, L., Pompili, M., Sangiovanni, S., Baur, M. and Knauel, J., 2018, October. Standard evolution for the determination of the power frequency breakdown voltages in insulating liquids. In *2018 IEEE Conference on Electrical Insulation and Dielectric Phenomena (CEIDP)* (pp. 263-266). IEEE.

6. ASTM C1161 − 18Jenkins, M. G., Salem, J. A., Helfinstine, J., Quinn, G. D., & Gonczy, S. T. (2017). International Standards for Properties and Performance of Advanced Ceramics–30 Years of Excellence. *Mechanical*

Properties and Performance of Engineering Ceramics and Composites XI: Ceramic Engineering and Science Proceedings Volume 37, Issue 2, *37*, 1-12.

7. ASMT C1327 − 15 Shamsudin, Z., & Mesri, M. (2022). Investigation on performance of eco-waste composite materials via Vickers and acoustic measurement. *Proceedings of Mechanical Engineering Research Day 2022*, *2022*, 97-98.

8. ASTM C1421 − 18 Swab, J. J., Tice, J., Wereszczak, A. A., & Kraft, R. H. (2015). Fracture toughness of advanced structural ceramics: applying ASTM C1421. *Journal of the American Ceramic Society*, *98*(2), 607-615.

9. ASMT C1424 − 15 Sirivivatnanon, V., Thomas, P., Tapas, M. J., & Nguyen, T. N. (2023). Reliability of AMBT and CPT in testing the effectiveness of SCM to mitigate alkali–silica reaction of field concrete. *Construction and Building Materials*, *369*, 130510.

10. Kini, A. U., Shettar, M., Gowrishankar, M. C., & Sharma, S. (2023). A technical review on epoxy-nanoclay nanocomposites: Mechanical, hygrothermal and wear properties. *Cogent Engineering*, *10*(2), 2257949.

11. Badachi, C and Dixit, P(2016). Predictions of pollution flashover voltages of ceramic string insulators under uniform and non-uniform pollution conditions. *Journal of Electrical systems and information Technology.* **3**, pp 270-281

12. Ban, S. (2021). Classification and properties of dental zirconia as implant fixtures and superstructures. *Materials*, *14*(17), 4879.

13. Freiman, S. W., & Mecholsky Jr, J. J. (2019). *The fracture of brittle materials: testing and analysis*. John Wiley & Sons.

14. Barbachi, M., Imad, A., Jeffali, F., Boudjellal, K., and Bouabaz, M. (2017). Physical Characterization of Seashell for a Concrete Formulation. *Journal of Materials and Environment Sciences.* **8**(1), pp. 332-337.

15. Ansari, A. I., Sheikh, N. A., & Kumar, N. (2024). Visco-mechanical characterization of Molluscs (sea shell) biomimetics designs structures. *Journal of the Brazilian Society of Mechanical Sciences and Engineering*, *46*(5), 326.

16. Bonou, S. S., Sagbo, E., Aubry, C., Charvillat, C., Ben-Nissan, B., & Cazalbou, S. (2019). Conversion of snail shells (Achatina achatina) acclimatized in Benin to calcium phosphate for medical and engineering use. *Journal of the Australian Ceramic Society*, *55*(4), 1177-1186.

17. Buranyi, S. (2015) Snail Shells are Inspiring Tomorrow's Toughest Materials. *MOTHERBOAD, McGill UniversityPress. London.*

18. Odusanya, A. A., Bolasodun, B., Madueke, C. I. (2014). Property Evaluation of Hybrid Seashell/Snail shell Filler Reinforced Unsaturated Polyester Composite in Comparison with Seashell and Snail Shell Filler Reinforced Unsaturated Polyester Composite. *The International Journal of Engineering and Science.* **3**(12), pp 80 – 90

19. Tiwari, F. (2024). Ecofriendly Management of Giant African Snail (GAS) Achatina fulica (Bowdich). *Journal Nutrition and Food Processing*, *7*(4).

20. Tobins, F. H., Abubakre, O. K., Muriana, R. A., & Abdulrahman, A. S. (2018). Snail shell as an inspiring engineering material in science and technology development: a review. 20408-20416. 10.15520/ijcrr/2018/9/03/473.

21. Thiengo, S. C., Maldonado, A., Mota, E. M., Torres, E. J. L., Caldeira, R., Carvalho, O. S., ... & Lanfredi, R. M. (2010). The giant African snail Achatina fulica as natural intermediate host of Angiostrongylus cantonensis in Pernambuco, northeast Brazil. *Acta tropica*, *115*(3), 194-199.

22. Yigezu, B. S., Mahapatra, M. M., Jha, P. K. (2013) Influence of Reinforcement Type on Microstructure, Hardness and Tensile properties of an Aluminium Alloy Metal Matrix Composites. *Journal of Minerals and Materials Characterization and Engineering.* 1, 124 - 130.